J. Micromech. Microeng. **10** (2000) 34–41. Printed in the UK PII: S0960-1317(00)06838-8

The effect of residual stresses on the deformation of semi-circular micromachined beams

Chingfu Tsou and Weileun Fang

Power Mechanical Engineering Department, National Tsing Hua University, Hsinchu, Taiwan

Received 11 August 1999

Abstract. In this research, a semi-circular micromachined beam is proposed in order to reduce the out-of-plane deformation caused by the residual stresses. The side view of the semi-circular beam is similar to that of a cantilever, whereas the end conditions are similar to those of the microbridge. Although the micromachined cantilever will not be deformed by the residual mean stress, it is significantly bent by the residual gradient stress. On the other hand, the microbridge will not be bent by the gradient residual stress, but is buckled by the mean compression. Analytical and experimental results demonstrate that the out-of-plane deformation due to bending and buckling is significantly reduced for the semi-circular micromachined beam. Thus, the flatness of the micromachined suspensions is improved. The more traditional techniques in which the out-of-plane deformation is reduced, by lowering the net residual stresses of thin films, can be supplemented by the use of the semi-circular micromachined beam.

1. Introduction

Silicon micromachining is an advanced technology that is used to fabricate tiny mechanical structures through thin-film processes. Due to the mismatch of thermal expansion coefficients between the materials as well as the imperfections that accumulate in them, significant residual stresses normally exist in the thin films. Consequently, thin-film residual stresses can be categorized as thermal stress and intrinsic stress [1]. The residual stresses will cause undesired out-of-plane deformation of the micromachined structures, such as bending and buckling [2]. Therefore, the mechanical properties of the micromachined structures, such as stiffness and resonant frequencies, could be directly affected [3]. In addition, optical properties, such as the mirror flatness of a micromachined plate, are indirectly influenced by the residual stresses [4]. In short, it is important to consider the residual stress effect while designing micromachined devices.

Due to the restriction in silicon micromachining processes, there are a limited number of micromachined structures available. Presently, the micromachined cantilever [5, 6] and bridge [7] (microbridge) are the most common structures used for thermal isolation [8–10] as well as suspension [11, 12]. Applications for these devices include the chemical sensor [9], fluidic sensor [10], atomic force microscope [11] and accelerometer [6, 12]. Since thermal oxide and stoichiometric nitride are often used to fabricate the above structures, the microbeams are subjected to large residual stresses. Thus, the microcantilever will be bent by the residual stress due to its small bending stiffness [13]. In contrast, the microbridge will be buckled by the residual stress [14]. Currently, two approaches have been proposed to reduce the out-of-plane deformation of the micromachined structures induced by the residual stresses [15–17]. First, the thin-film

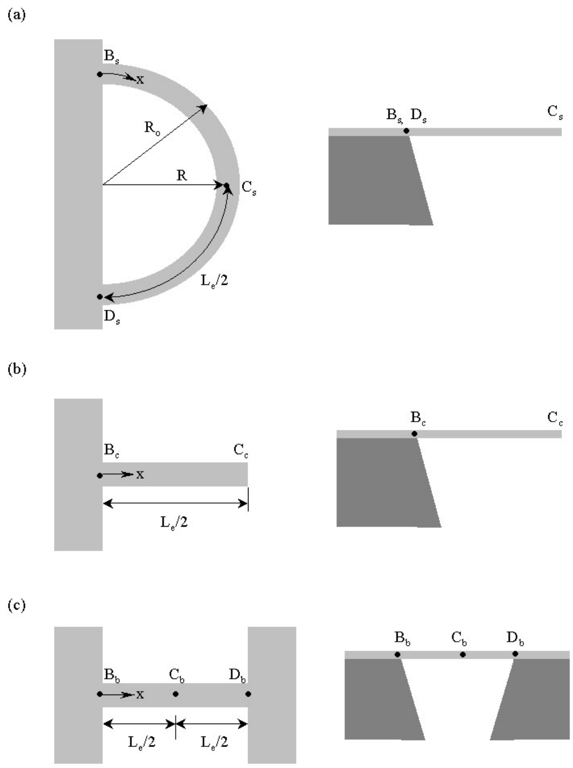

Figure 1. The schematic view of three different micromachined beams, (a) the semi-circular microbeam, (b) the microcantilever and (c) the microbridge.

0960-1317/00/010034+08$30.00

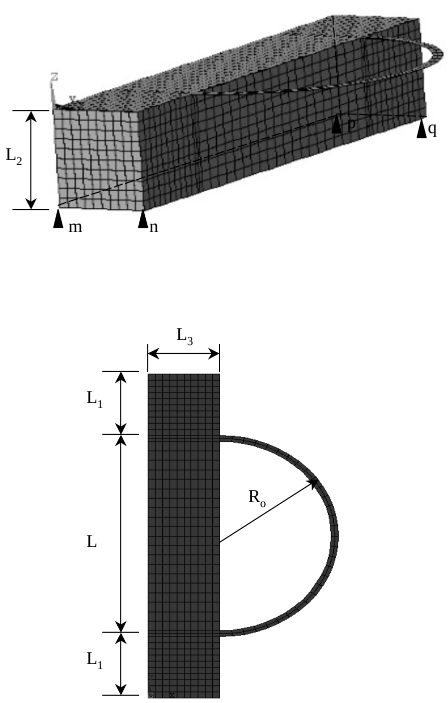

Figure 2. The three-dimensional FEM established in this study.

residual stresses are minimized by either optimizing the thin-film deposition conditions or using heat treatments [15]. Second, the net bending moment induced by the residual stresses is compensated by using multilayer thin films [16, 17]. However, the thin-film materials available as well as the fabrication processes for these two approaches are limited.

In this research, a semi-circular micromachined beam (microbeam) is proposed to reduce the out-of-plane deformation caused by the residual stresses. The flatness of the micromachined beams are improved without changing the thin-film materials or the fabrication processes. As shown in figures 1(a) and 1(b), the side view of the semi-circular microbeam is similar to that of the microcantilever, while the end conditions are similar to that of the microbridge, as shown in figures 1(a) and 1(c). A finite-element model (FEM) was established to predict the effect of the residual stresses on the semi-circular beam. In addition, an array of semi-circular microbeams with various thicknesses, widths and radii were fabricated and characterized. As demonstrated through the analytical and experimental results, the flatness of the micromachined beams is remarkably improved by the semi-circular design.

2. Theoretical analysis

For the first approximation, the residual stresses of a thin film can be regarded as [2]

$$\sigma_{total} \approx \sigma_0 + \sigma_1 \left(\frac{2y}{h}\right) \tag{1}$$

where h is the thickness of the thin film and $y \epsilon (-h/2, h/2)$ is the coordinate across the thickness, with its origin at the mid-plane of the film. From equation (1), the residual

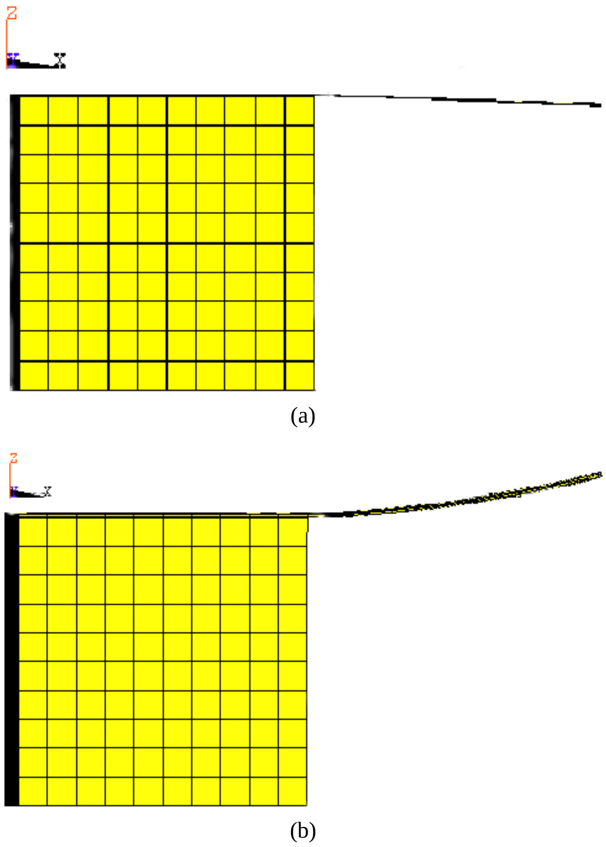

Figure 3. The side view of the finite-element analysis results regarding the configurations of the semi-circular microbeam deformed by (a) the mean residual stress and (b) the gradient residual stress.

stresses are comprised of a mean component σ_0 and a gradient component σ_1. Therefore, the buckling of the microbridge is induced by the mean compressive residual stress, and the bending of the microcantilever is caused by the gradient residual stress. In this section, the out-of-plane deformation led by the mean stress and gradient stress on the semi-circular microbeam is studied. The deformation configuration of the semi-circular microbeams is predicted by a FEM. In addition, the deformation amplitudes of the microcantilever, microbridge and semi-circular microbeam are also discussed. The microcantilever has a maximum deflection at the tip of the beam, whereas the microbridge and the semi-circular microbeam have a maximum deflection at the middle of the beam. The lengths of the beams, discussed in this study, are $L_e/2$, L_e and L_e, for the microcantilever, the microbridge and the semi-circular microbeam, shown respectively in figure 1. The equivalent length L_e of the beam is $L_e = \pi R/2$.

A three-dimensional FEM shown in figure 2 was established to simulate the semi-circular microbeam and its boundaries. This model includes a semi-circular microbeam and its underlying silicon substrate. Semi-circular microbeams with thickness $h = 1$ μm, width $w = 5$ μm and varying radii ($R_0 = 25$– 95 μm) were analyzed. The silicon substrate used in the experiment was 500 μm thick. The thickness L_2 of the substrate modeled in figure 2 would not influence the results of the finite-element analysis

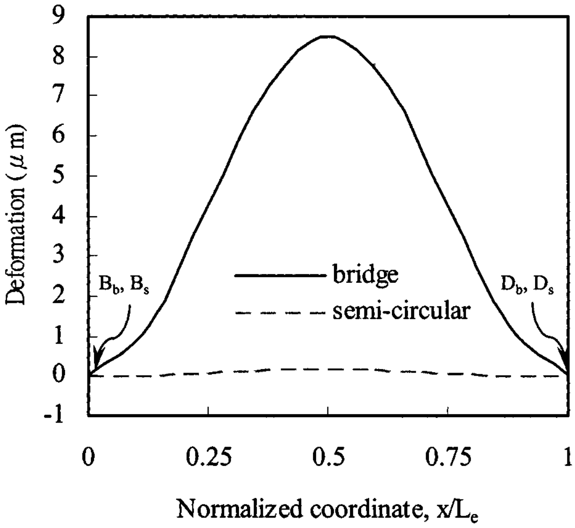

(a)

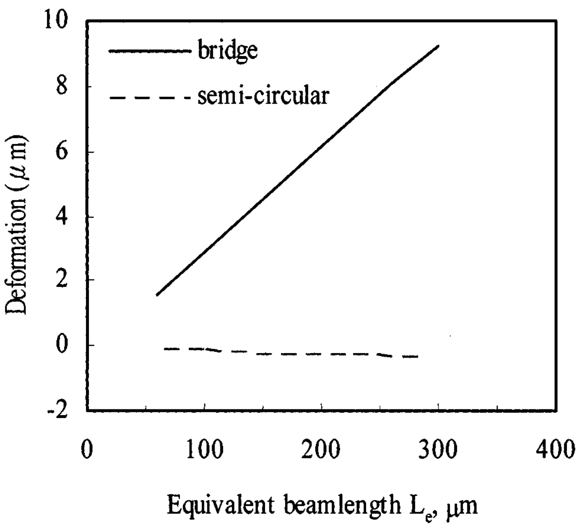

(b)

Figure 4. (a) The deformation configurations and (b) the variation of the deflection amplitude against beam length, of the microbridge and semi-circular microbeam.

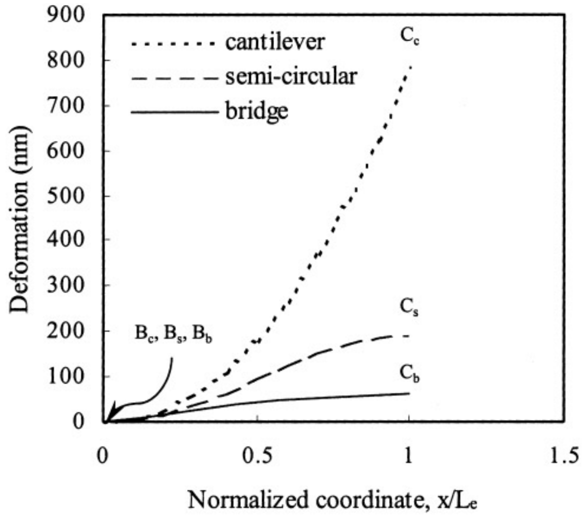

(a)

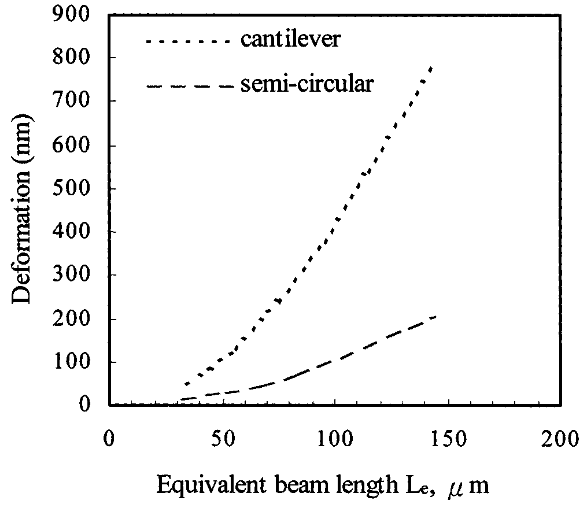

(b)

Figure 5. (a) The deformation configurations and (b) the variation of the deflection amplitude with beam length, of the microbridge, microcantilever and semi-circular microbeam.

if L_2 exceeds 100 μm. Thus, the thickness L_2 in the FEM was only 100 μm instead of 500 μm in order to save the computational time. Similarly, the wall thicknesses L_1 and L_3 were modeled to be 100 μm instead of several millimeters. The material applied in the FEM was thermal SiO_2, to allow for comparison with the experimental results. The residual stresses of the thin films were determined using the technique presented in [2]. The elastic modulus of SiO_2 and Si were respectively taken to be 73 GPa and 190 GPa [18], and the Poisson's ratios of SiO_2 and Si were assumed to be 0.17 and 0.27, respectively.

2.1. Mean residual stress effects

The mean residual stress σ_0 has two effects on the semi-circular microbeam: the boundary effect and the domain effect. As to the boundary effect, the boundary conditions of a micromachined beam are different from those of the conventional beam [2]. For instance, the microcantilever has an angular deflection due to its deformed boundary. According to the FEM results, a typical side view of the semi-circular microbeam under mean residual stress σ_0 is shown in figure 3(a). Likewise, the semi-circular microbeam has an angular deflection due to the boundary effect.

As to the domain effect, the microbridge shown in figure 1(c) will be buckled when applied by a certain residual compression σ_0. However, the semi-circular microbeam, which has the same cross-section and length as those of the microbridge, subjected to the same load σ_0 does not buckle. The typical analytical results of the out-of-plane deformation configurations for a microbridge and a semi-circular microbeam are presented in figure 4(a). The horizontal axis represents the normalized coordinate x/L_e along the beam length. From the FEM result, the deflection profile of a $R_0 = 95$ μm semi-circular beam along its circumference is given by the dashed curve in figure 4(a). The full curve in figure 4(a) indicates the deflection profile of the microbridge which has an equivalent length $L_e = \pi R$. The microbridge is buckled in this manner, yet the semi-

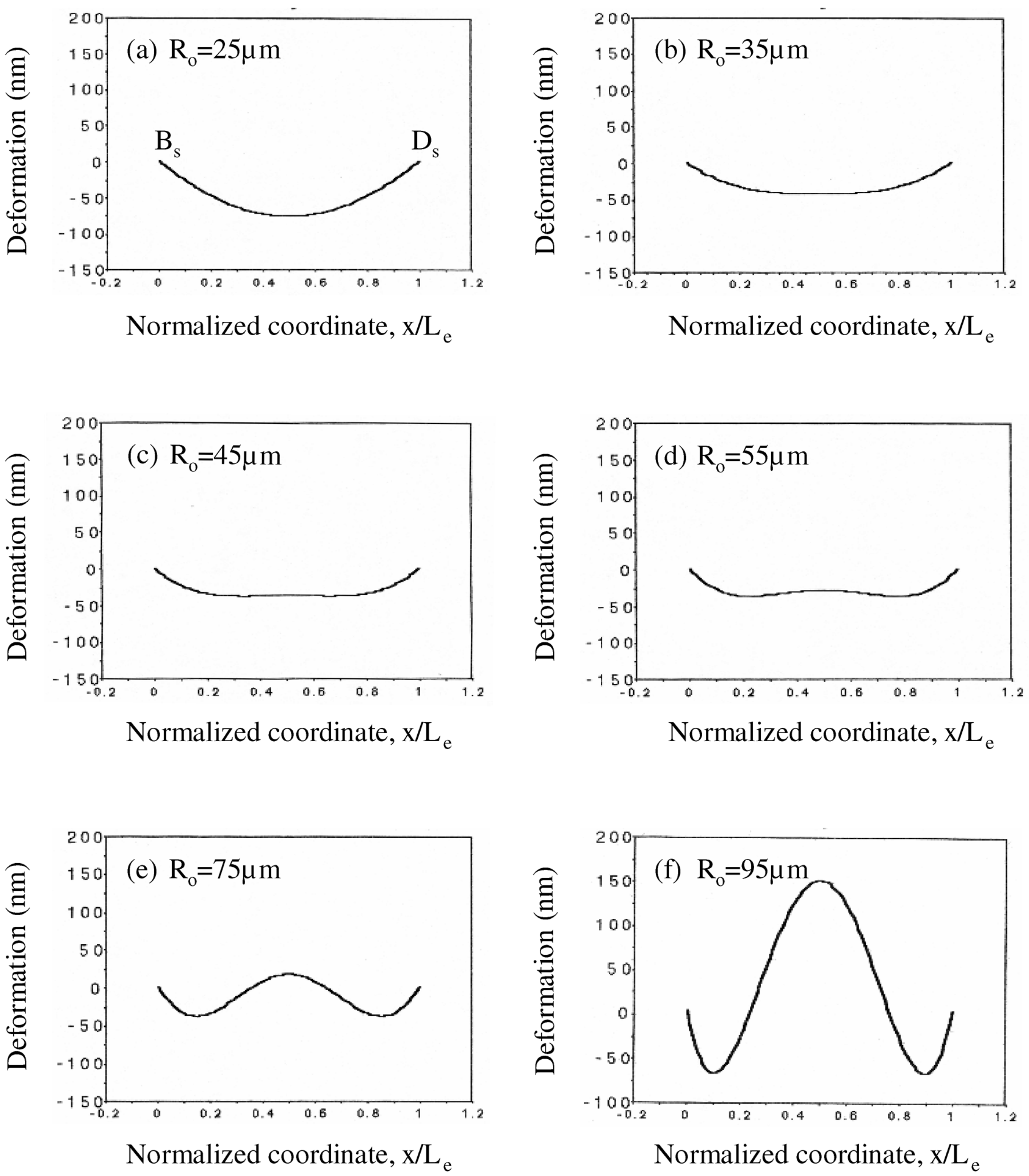

Figure 6. The predicted deflection configurations of six different length semi-circular microbeams along their circumference. These microbeams are under both the mean and the gradient residual stresses.

circular microbeam is not buckled. Consequently, the out-of-plane deformation amplitude of the microbridge is 56 times greater than that of the semi-circular microbeam. In other words, the proposed semi-circular microbeam can be used to prevent the micromachined structures from being buckled by the mean residual stress σ_0.

The deflection amplitude of the microbridge and the semi-circular beam for various equivalent beam lengths L_e were also analyzed in this study. Figure 4(b) shows the variation of the deflection amplitude with the equivalent beam length L_e for semi-circular beam and the microbridge. It is clear that the deflection amplitude of the microbridge changes remarkably with L_e. On the other hand, the deflection amplitude of the semi-circular microbeam stays fairly constant for different L_e.

2.2. Gradient residual stress effect

According to equation (1), the micromachined beams are also under a bending moment which arises from the gradient residual stress. As predicted by the FEM, the side view of a semi-circular beam after being deformed by a gradient residual stress is shown in figure 3(b). In this manner, the typical analytical results of the out-of-plane deformation configurations of a microbridge, a semi-circular microbeam and a microcantilever, respectively, are shown in figure 5(a). The curves shown in figure 5(a) are the deflection profiles between the points B and C indicated in figure 1. The dashed curve represents the deformation configuration of a semi-circular microbeam along its circumference B_sC_s whose radius $R_0 = 95\ \mu$m. The deflection amplitude of the semi-circular beam at point C_s is 0.18 μm. In addition, the full

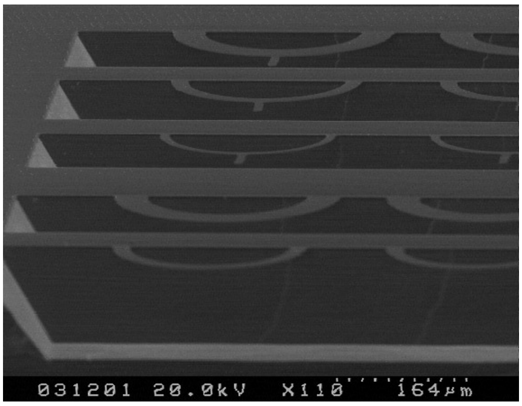

Figure 7. The SEM photograph of the semi-circular microbeams.

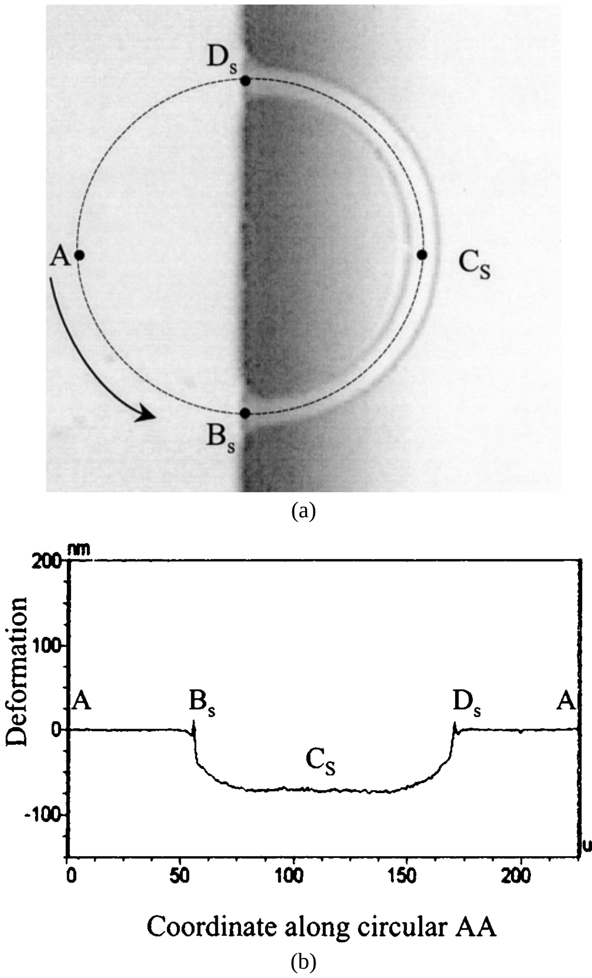

Figure 8. (a) The optical microscope photograph of the 1.0 μm thick SiO_2 semi-circular microbeam to be measured and (b) the measured deflection profile of the beam shown in (a) along the path A $\rightarrow$ B_s $\rightarrow$ C_s $\rightarrow$ D_s $\rightarrow$ A.

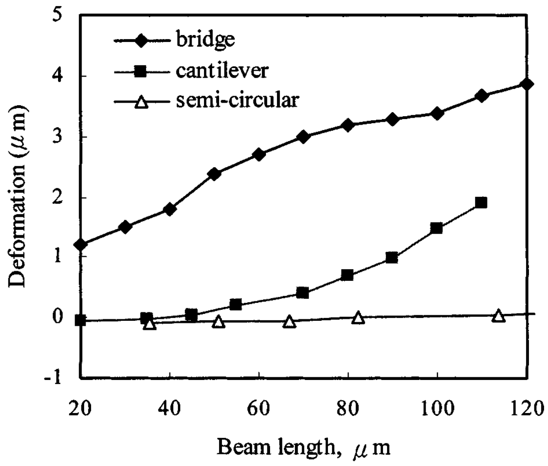

Figure 9. The measured deflection amplitudes of the 1.0 μm thick SiO_2 semi-circular microbeams, microcantilevers and microbridges against beam length.

curve indicates the deformation configuration of a straight microbridge along B_bC_b. The deflection amplitude of the microbridge at point C_b is only 0.05 μm. The dotted curve depicts the deformation configuration of a microcantilever along B_cC_c. The deflection amplitude of the microcantilever at point C_c is 0.8 μm. Thus, the out-of-plane deflection of the semi-circular microbeam is 4.5 times smaller than that of the microcantilever. According to the analysis, the semi-circular microbeam significantly reduces the out-of-plane deflection induced by the gradient residual stress. It is concluded that the design of the semi-circular microbeam can also be used to prevent micromachined structures from being bent by the gradient residual stress σ_1.

The deflection amplitude of the microcantilever and the semi-circular beam for various L_e were also analyzed. As illustrated in figure 1, the length of the microcantilever is $L_e/2$ and the length of the semi-circular beam is L_e. The variation of the bending amplitude with L_e for the semi-circular beam and the microbridge is shown in figure 5(b). In comparison with the semi-circular microbeam, the deflection amplitude of the microcantilever changes remarkably with the variation of L_e. Thus, the semi-circular microbeam can significantly reduce the out-of-plane deformation induced by either mean or gradient residual stresses.

2.3. Net effect

The net deformation of semi-circular microbeams caused by the residual stresses is obtained by superposing the effects of the mean residual stress and the gradient residual stress. According to the result from the FEM analysis, the net deformation profiles of the semi-circular microbeams with six different radii are shown in figure 6. These deflection profiles were measured along the circumference B_sD_s of the semi-circular microbeam shown in figure 1(a). As indicated in figure 6(a), the semi-circular microbeam tilts downward when R_0 is equal to 25 μm. Hence, the deformation of the shorter beam is dominated by the boundary effect induced by the mean residual stress. According to the bending effect led by the gradient residual stress, the middle region of the beam became flat when R_0 was equal to 35 μm, as shown in figure 6(b). The middle region of the semi-circular microbeam gradually deflected upward when R_0 increased from 45 μm to 95 μm, as shown in figures 6(c)–6(f). In other words, the deformation of the longer beam is dominated by the bending effect induced by the gradient residual stress.

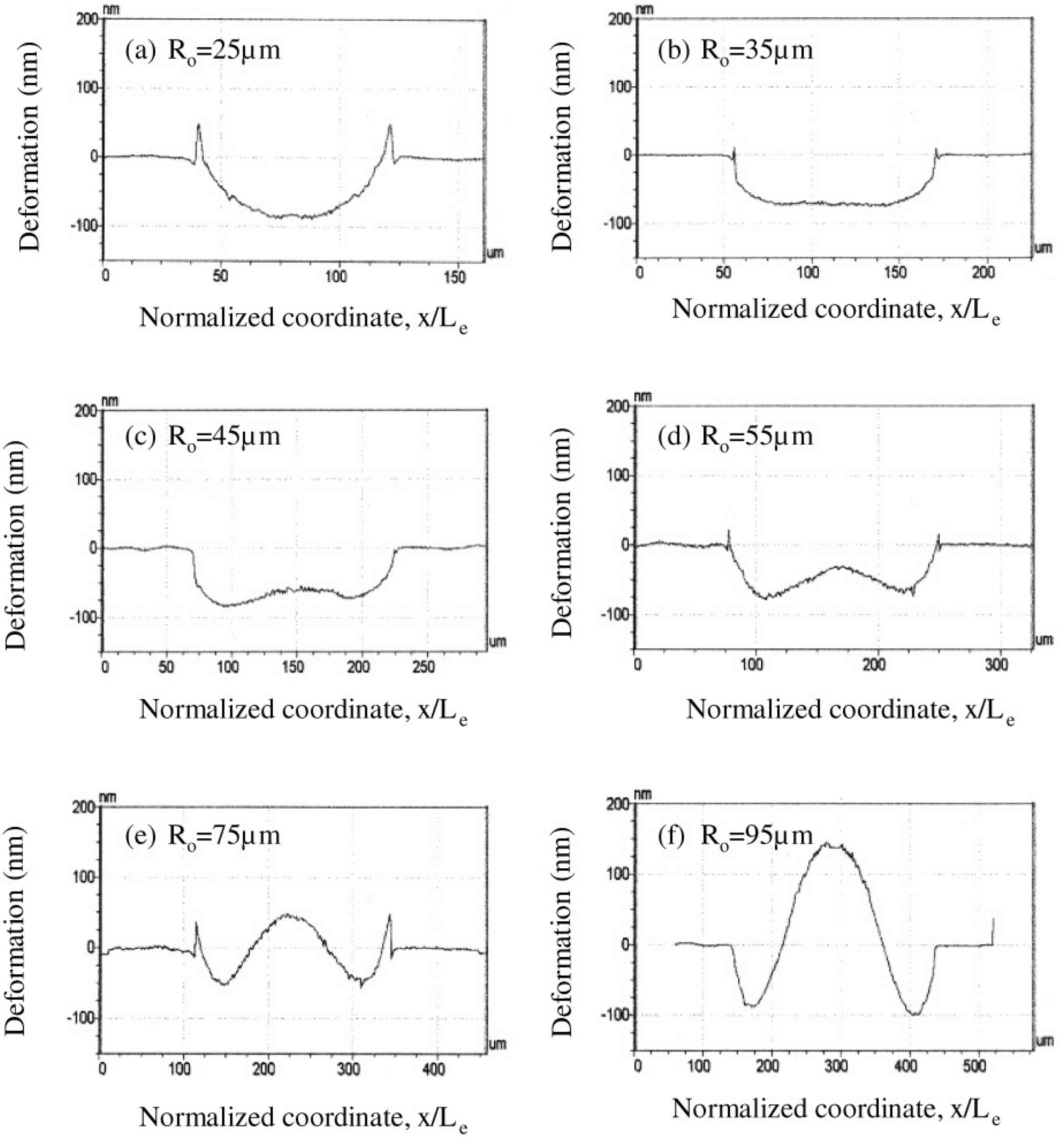

Figure 10. The measured deflection configurations of six different length semi-circular microbeams along their circumference. These microbeams are under both the mean and the gradient residual stresses.

3. Experiment and results

In this experiment, the SiO_2 semi-circular microbeams with nine different radii R_0 between 15 μm and 95 μm were fabricated by bulk micromachining. Three different beam widths (5, 10 and 15 μm) were used for each beam radius. the (100) single crystal silicon is the substrate material in the experiment. The single crystal silicon was placed in the furnace to grow a 1 μm thick thermal oxide layer at 1050 °C. After the substrate was etched anisotropicly by KOH, the micromachined beams were suspended. The scanning electron microscope (SEM) photograph of typical semi-circular microbeams is shown in figure 7. In the experiment, the micromachined beams were deformed by the residual stresses of the thermal oxide. In order to compare the deflection among different micromachined beams, the microbridges with lengths of 20–120 μm, and microcantilevers with lengths from 10 μm to 110 μm were also fabricated.

To determine the influence of residual stresses on the semi-circular microbeams, the out-of-plane deformation configurations of the semi-circular beams were measured by the interferometric profilometry. A typical measured result is shown in figure 8. The optical microscope photograph shown in figure 8(a) is the top view of the region measured by the profilometry. The region at the left side of B_sD_s is still bonded to the substrate. On the other hand, the semi-circular beam at the right side of B_sD_s is suspended above a cavity. The surface profile measured along the circular path A $\rightarrow$ B_s $\rightarrow$ C_s $\rightarrow$ D_s $\rightarrow$ A indicated by the dashed line in figure 8(a) is shown in figure 8(b). The out-of-plane deformation configuration of the semi-circular microbeam is indicated by the dip marked by $B_sC_sD_s$ in figure 8(b). In addition, the deflection amplitude at the point C_s was determined. In the same manner, the deflection amplitude of the cantilever and the microbridge at the points C_c and C_b were also determined.

The measured out-of-plane deformation amplitudes of the SiO_2 microbeams at the points C_s, C_c and C_b, are shown in figure 9. The length of microbridge ranges from 30 μm to 120 μm, and the buckling amplitude caused by the mean stress is from 1.5 μm to 3.9 μm. As the beam length increases, the buckling amplitude at C_b increases, while the increment of the deformation amplitude gradually decreases. In addition, the length of the microcantilever ranges from 35 μm to 110 μm, and the bending amplitude caused by the gradient stress is from -0.037 μm to 1.9 μm. However, the increment of the deformation amplitude at C_c drastically increases with increasing beam length. The length of the semi-circular microbeam ranges from 35 μm to 145 μm, and the out-of-plane deformation caused by the residual stresses is from -0.14 μm to 0.15 μm. Experimental results show that the out-of-plane deformation of the semi-circular microbeam is approximately one to two orders of magnitude smaller than that of the microcantilevers and microbridges.

In order to make a comparison with the analytical results, the measured deformation configurations of the semi-circular microbeams for six different radii are shown in figure 10. As indicated in figure 10(a), the semi-circular microbeam with a radius $R_0 = 25$ μm tilts downward. The middle region of the beam gradually deflects upward when R_0 increases from 35 μm to 95 μm, as shown in figures 10(b)–10(f). Therefore, it is observed that for shorter beams the deformation configuration of a semi-circular beam is dominated by the mean residual stress. As the beam length increases, the deformation configuration becomes dominated by the gradient residual stress. In short, the deformation profiles of the semi-circular beam for various beam lengths predicted by the FEM agree qualitatively with those measured from the experiment.

4. Discussion and conclusion

The micromachined beams are normally subjected to the loading of residual stresses. Although the microcantilever will not be deformed by the mean compression, it is bent significantly by the residual gradient stress. On the other hand, the microbridge will not be bent by the gradient residual stress, but it will be buckled by the mean compression. In this study, the semi-circular microbeam design is intended to improve the existing micromachined suspensions. It has been demonstrated through the analytical and experimental approaches that the semi-circular microbeam can drastically reduce the out-of-plane deformation induced by the residual stresses. Thus, the more traditional techniques, in which the out-of-plane deformation is reduced by lowering the net residual stresses of thin films, can be supplemented by the use of a semi-circular beam.

The etching time required to fully undercut the semi-circular microbeam is less than that for the microcantilever. The etching time for a $L_e = 300$ μm semi-circular beam is 30 min while the etching time for a 150 μm long microcantilever is more than 45 min. Apparently, the thickness of the thin film suffers less attack during etching for a semi-circular beam. In addition, the semi-circular microbeam has a better film-thickness uniformity.

The deflection profile of the semi-circular microbeam measured in the experiment supports the FEM established in this study. The FEM in this manner can be applied to the prediction of the deflection amplitude as well as the deflection profile for semi-circular beams of different lengths. Semi-circular microbeams with specified out-of-plane geometries can be designed, provided that their deflection profiles can be predicted from the model.

Acknowledgments

This paper was originally published in the ASME Proceedings of the 1999 International Mechanical Engineering Congress and Exhibition (IMECE), Nashville, TN. This material is based (in part) upon work supported by the National Science Council (Taiwan) under Grant NSC 88-2218-E007-004. The author would like to express his appreciation to the Electrical Engineering Department of National Tsing Hua University (Taiwan), Semiconductor Center of National Chiao Tung University (Taiwan) and National Nano Device Laboratories (Taiwan) in providing fabrication facilities.

References

[1] Thornton J A and Hoffman D W 1989 Stress-related effects in thin film *Thin Solid Films* **171** 5–31

[2] Fang W and Wickert J A 1996 Determining mean and gradient residual stresses in thin films using micromachined cantilevers *J. Micromech. Microeng.* **6** 301–9

[3] Zhang L M, Uttamchandani D, Culshaw B and Dobson P 1990 Measurement of Young's modulus and internal stress in silicon of microresonators using a resonant frequency technique *Meas. Sci. Technol.* **1** 1343–6

[4] Hsieh J and Fang W 1998 Fabrication of micro torsional actuator using surface plus bulk micromachining processes *Proc. SPIE* **3514** 368–76

[5] Shoji S and Esashi M 1994 Microflow devices and systems *J. Micromech. Microeng.* **4** 154–71

[6] Brugger J, Buser R A and de Rooij N F 1992 Silicon cantilevers and tips for scanning force microscopy *Sensors Actuators* A **34** 193–200

[7] Gajda M A and Ahmed H 1995 Applications of thermal silicon sensors on membranes *Sensors Actuators* A **49** 1–9

[8] Volklein F and Baltes H 1992 A microstructure for measurement of thermal conductivity of polysilicon thin films *J. Microelectromech. Syst.* **1** 193–6

[9] Norlin P, Ohman O, Ekstrom B and Forssen L 1997 A chemical micro analysis system for measurement of pressure, flow rate, temperature, conductivity, UV-absorption and fluorescence *Int. Conf. on Solid-State Sensors and Actuators (Chicago, IL 1997)* pp 507–10

[10] Neda T, Nakamura K and Takumi T 1995 A polysilicon flow sensor for gas flow meters *8th Int. Conf. on Solid-State Sensors and Actuators and Eurosensors IX (Stockholm, Sweden)* pp 548–55

[11] Liu C and Gamble R 1998 Mass-producible monolithic silicon probes for scanning probe microscopes *Sensors Actuators* A **71** 233–7

[12] Noworolski J M, Klaassen E H, Logan J R, Petersen K E and Maluf N I 1996 Process for in-plane and out-of-plane single-crystal-silicon thermal microactuators *Sensors Actuators* A **55** 65–9

[13] Lin H-Y and Fang W 1998 Design and fabrication of a microvalve with an anti-leakage membrane *6th Int. Conf. on Micro Electro, Opto, Mechanical Systems and Components (Potsdam, Germany, December, 1998)* pp 325–30

[14] Fang W and Wickert J A 1994 Post buckling of micromachined beams *J. Micromech. Microeng.* **4** 116–22
[15] Zhang X, Zhang T Y, Wong M and Zohar Y 1998 Residual-stress relaxation in polysilicon thin films by high-temperature rapid thermal annealing *Sensors Actuators* A **64** 109–15
[16] Chou B C S, Shie J-S and Chen C-N 1997 Fabrication of low-stress dielectric thin-film for microsensor applications *IEEE Electron Device Lett.* **18** 599–601
[17] Volklein F 1990 Thermal conductivity and diffusivity of a thin film SiO_2–Si_3N_4 system *Thin Solid Films* **188** 27–33
[18] Petersen K E 1982 Silicon as a mechanical material *Proc. IEEE* **70** 420–57